Integration of GPS, Radar Interferometry and GIS for Ground Deformation Monitoring

Linlin Ge, Hsing-Chung Chang, Volker Janssen, and Chris Rizos
Satellite Navigation And Positioning Group
School of Surveying & Spatial Information Systems
The University of New South Wales
Sydney NSW 2052, AUSTRALIA
Email: l.ge@unsw.edu.au

BIOGRAPHY

The authors are all with the School of Surveying and Spatial Information Systems at the University of New South Wales, Sydney, Australia. Linlin Ge is a Research Fellow and leader of InSAR and deformation monitoring research programs. He is co-chair of Sub-Commission 4.4 "Applications of Satellite and Airborne Imaging Systems" of the International Association of Geodesy (IAG). Hsing-Chung Chang is a PhD candidate. Volker Janssen is an Associate Lecturer. Chris Rizos is a Professor and the leader of the Satellite Navigation And Positioning Group. He is also the President of Commission 4 "Positioning & Applications" of the IAG.

ABSTRACT

Dense continuously-operating networks of GPS receivers (CGPS) have been established in many parts of the world in order to monitor ground deformation due to earthquakes and other activities. However, it has been found that the CGPS is still NOT dense enough to monitor some phenomena, e.g. volcano and ground subsidence due to mining. Therefore the authors propose to combine GPS with radar interferometry (InSAR) and GIS so that CGPS can monitor small scale deformation as well. The methodology is to use CGPS to estimate the differential tropospheric delays and apply these estimations as corrections to the radar interferometric results in order to ensure sub-centimetre accuracy. The corrected InSAR results are exported to the GIS so that the ground deformation can be interpreted along with other spatial information such as aerial photos and mine plans. Data from both the SCIGN and GEONET have been employed to test the tropospheric estimation process. InSAR results for monitoring subsidence due to underground mining in an Australian region have been interpreted with the aid of the GIS.

1. INTRODUCTION

Continuously-operating GPS networks consisting of state-of-the-art, dual-frequency receivers have been established in many parts of the world (e.g. Bock et al., 1993; Miyazaki et al., 1996) to support geodynamic studies, on a range of spatial scales. These include tracking surface crustal deformation on local and regional scales associated with active seismic faults and volcanoes, local monitoring of slope stability (caused by open pit mining operations, unstable natural features, etc.), and measuring ground subsidence over small areal extents (due to underground mining, extraction of fluids, etc.). Current GPS capabilities permit the determination of inter-receiver distances at the sub-cm accuracy level (typically on a daily basis) for receiver separations of tens to hundreds of kilometres, from which can be derived the rate-of-change of distance between precisely monumented groundmarks. This is the basic geodetic measure from which can be inferred the ground deformation. The pattern of ground deformation determined from the analysis of such measures across a CGPS network is an important input to models that seek to explain the mechanisms for such deformation, and hopefully to mitigate the damage to society caused by such (slow or fast) ground movements.

The Japanese GEONET (GSI, 2003) and the SCIGN (2003) in the western USA are among the first CGPS networks. Many more countries and regions are expanding their own CGPS networks, such as China, South Korea, Taiwan, Hong Kong, Germany, U.K., Singapore, Russia, to name but a few. Data from CGPS arrays are also used in meteorological research projects to test the feasibility of operational mapping of the tropospheric water vapour, and for the study of ionospheric disturbances.

However, for many geodynamic applications these CGPS arrays of receivers are not capable, on their own, of determining the characteristics of crustal motion at the fine temporal or spatial scales required. For example, although the spatial resolution of Japan's GEONET, the

largest and best instrumented of the CGPS networks, consisting of over 1000 stations, is now as high as about 30km, because of the high cost of dual-frequency GPS receivers they may not be established in a dense enough configuration to address all geodetic or geodynamic applications. In fact, if one inspects the resolution requirements for some geophysical and geological applications (as shown in Fig. 1, where the coverage of the current CGPS is indicated by the dashed-line rectangle), the requirements for a majority of the applications remain unsatisfied. If the rectangle is extended in the negative direction of the vertical axis, this represents a 'temporal densification of the GPS measurements'. If the rectangle is extended in the negative direction of the horizontal axis, this is a 'spatial densification of the GPS measurements' (Ge, 2000). While it is straightforward to realise these temporal and spatial densifications by increasing the data sampling rate on the one hand, and by deploying many more GPS receivers on the other hand, it is not generally economically feasible to do so.

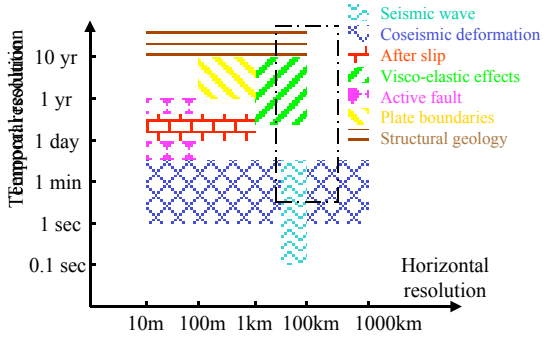

Figure 1 Resolution requirements of some geophysical and geological applications (various sources).

Interferometric Synthetic Aperture Radar (InSAR), on the other hand, exhibits around 25m spatial resolution. But InSAR is very sensitive to errors such as atmospheric effects (tropospheric delay, ionospheric delay, etc., Zebker et al., 1997), satellite orbit error, condition of the ground surface and temporal decorrelation. When present in the InSAR image, these errors can be very misleading and result in misinterpretation. Since data from CGPS arrays can be used to map tropospheric water vapour and ionospheric disturbances, these results can be used to remove atmospheric effects in InSAR.

Therefore it is obvious that the two techniques are complementary. Furthermore, Geographic Information Systems (GIS) have been widely used in many organisations, such as local council, government, real estate, transport authority, etc. GIS has evolved into an important tool for the management of land information, urban information, natural resource information, and so on (Bernhardsen, 2002). Exporting InSAR results into a GIS, and post-processing them along with other GIS data layers such as aerial photos and mine plans makes the interpretation and archiving of them much easier. Therefore, it makes sense to add GIS to the combined GPS-InSAR system.

The rest of the paper is organised as follows: the second part discusses tropospheric corrections for InSAR derived from GPS observations; the third part is concerned with the interpretation of InSAR results with the aid of GIS; and the fourth part concludes the paper by summarising the findings.

2. TROPOSPHERIC CORRECTIONS FOR INSAR DERIVED FROM GPS OBSERVATIONS

2.1 GPS-derived tropospheric delay

The troposphere can be defined as the neutral (i.e. non-ionised) part of the atmosphere that stretches from the Earth's surface to a height of approximately 50km. The dominant impact of tropospheric path delay on radio signals occurs in the lower part, typically below 10km (Spilker, 1996). The tropospheric delay is dependent on temperature, atmospheric pressure and water vapour content. The tropospheric effect can be divided into two components, the dry and the wet component. The dry component accounts for about 90% of the effect and can be accurately modelled using surface measurements of temperature and pressure. However, due to the high variability of the water vapour content it is very difficult to model the remaining wet component.

Since the precise locations of CGPS sites can be estimated from long period observations (say 24 hours), and the ionospheric delay and dry tropospheric delay can be carefully eliminated or modelled, the residual variations of short period in the height can be attributed to the change of wet tropospheric delay. In this study the Bernese GPS processing software (Rothacher & Mervart, 1996) was used to derive tropospheric delay parameters for the individual stations of the network during parameter estimation. The user can specify the number of correction parameters to be estimated within the observation period.

2.2 Double-differencing algorithm for tropospheric delay corrections

Only the relative tropospheric delay (the tropospheric heterogeneity) between two SAR imaging points and between the two SAR image acquisitions will distort the deformation information derived by InSAR, because it is the phase difference that is used and deformation is always referenced to a stable point (site) in the image. Therefore, a between-site and between-epoch double-differencing algorithm can be used to derive the corrections to the InSAR result from GPS observations.

A. Single-differences

Assume that A is a stable site in the SAR image to be used as a reference point. B is another site in the same SAR image. If the tropospheric delay estimated from GPS for A and B at SAR imaging epoch j is denoted as D_A^j and D_B^j respectively, the between-site difference of the delays is:

$$D_{AB}^j = D_B^j - D_A^j \quad (1)$$

Using site A as the reference, single between-site difference delays at other GPS sites can also be calculated using equation (1), which are then interpolated (see next section) to generate a tropospheric delay image product similar to the radar SLC (single-look-complex) data.

B. Double-differences

Assuming two sites A and B, and two epochs j (master SLC image) and k (slave image), two single-differences may be formed according to equation (1):

$$\begin{aligned} D_{AB}^j &= D_B^j - D_A^j \\ D_{AB}^k &= D_B^k - D_A^k \end{aligned} \quad (2)$$

A double-difference is obtained by differencing these single-differences:

$$\begin{aligned} D_{AB}^{jk} &= D_{AB}^k - D_{AB}^j \\ &= (D_B^k - D_A^k) - (D_B^j - D_A^j) \\ &= (D_B^k - D_B^j) - (D_A^k - D_A^j) \end{aligned} \quad (3)$$

Equation (3) illustrates two possible approaches to double-differencing, either between-site (BS) differencing first and then between-epoch (BE) differencing (BSBE approach), or between-epoch differencing first and then between-site differencing (BEBS approach). The BSBE approach is preferred because the BS difference can be interpolated to generate a single-difference correction product. *This product will be associated with only the SLC image and hence can be used freely to form combinations for further BE differences as soon as InSAR pairs have been formed from SLC images.*

2.3 Interpolating tropospheric delay corrections

Continuous GPS networks may be as dense as one station every 25km at the national level, as is the case for the GEONET, or as dense as one station every few kilometres at the regional level, as is the case for the SCIGN. However, in order to correct the InSAR result on a pixel-by-pixel basis (ERS SAR resolution ~25m), the GPS-derived tropospheric corrections have to be interpolated. In this section the utility of three interpolating methods will be discussed.

A. Inverse distance weighted (IDW) interpolation

Inverse distance weighted interpolation (Lancaster & Salkauskas, 1986) explicitly assumes that things that are close to one another are more alike than those that are further apart. To predict a value for any unmeasured location, IDW will use the measured values surrounding the prediction location. Those measured values closest to the prediction location will have more influence on the predicted value than those farther away. Thus, IDW assumes that each measured point has a local influence that diminishes with distance, hence the name 'inverse distance weighted'.

B. Spline interpolation

This general-purpose interpolation method fits a minimum-curvature surface through the input points (Schultz, 1973). Conceptually, this is like bending a sheet of rubber to pass through the points while minimising the total curvature of the surface. It fits a mathematical function (a minimum-curvature, two-dimensional, thin-plate spline) to a specified number of the nearest input points while passing through all input points. Therefore, the idea behind a spline fit is to approximate a function by a polynomial which is defined piecewise. This method is best for gradually varying surfaces. It is not appropriate when there are large changes within a short horizontal distance because it can 'overshoot' estimated values. Hence, it would not be applicable to correct atmospheric interference induced by extreme weather conditions that may be caused by a cold front moving across the area.

C. Kriging interpolation

This interpolation method assumes that the distance or direction between sample points reflects a spatial correlation that can be used to explain variations in the surface. Kriging fits a mathematical function to a specified number of points, or all points within a specified radius, to determine the output value for each location. Kriging is a multistep process including exploratory statistical analysis of the data, variogram modelling, creating the surface, and (optionally) exploring a variance surface (Stein, 1999). This function is most appropriate when there is a spatially correlated distance or directional bias in the data.

2.4 Experimental data analysis: SCIGN

Data from the Southern California Integrated GPS Network (SCIGN, 2003) were used to investigate the feasibility of the above methods to derive tropospheric delay corrections from GPS observations. Of the 23 stations considered, 14 were treated as measured locations

(reference stations) and nine were used as prediction locations for which tropospheric delay corrections had to be determined and compared with their GPS-derived delays. A 2-hour session was observed on August 2, 2001 (DOY 214) and again on September 6, 2001 (DOY 249), simulating a typical ERS SAR satellite single repeat cycle of 35 days. Data were collected at a 30s sampling rate for a period of one hour before and after the flyover of the radar satellite. Figure 2 shows the location of the GPS sites within a typical ERS SAR image frame (the dashed lines) for this area, where the reference stations are denoted by triangles, while the sites to be interpolated are indicated by circles.

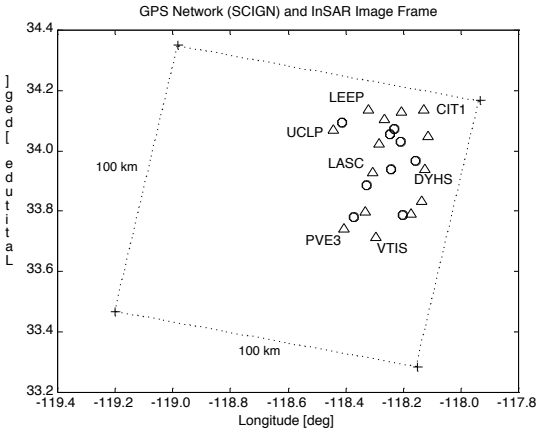

Figure 2. SCIGN stations within the ERS SAR image frame, showing reference stations (triangles) and prediction stations (circles)

The Bernese GPS processing software (Rothacher & Mervart, 1996) was used to process the network data from both days, the coordinates of CIT1 being held fixed as the primary reference station. Baseline lengths vary from 7km to 49km, and the largest height difference is 270m. For each site tropospheric delay corrections were determined every 20 minutes, resulting in six parameters per site throughout the 2-hour observation span. Single-differenced tropospheric corrections (equation (1)) were then obtained by forming the differences relative to CIT1. These corrections range from –6.1cm to +2.2cm, and in some cases show variations of a few centimetres within the 2-hour observation span.

Double-differenced tropospheric corrections are obtained by forming the between-epoch difference of the single-differenced values derived in the previous step (equation (3)). A comparison of the single- and double-differenced corrections revealed that almost all the double-differenced delay is smaller than the single-differenced delay (except for stations OXYC, MTA1 and PKRD). The double-differenced corrections range from –5.0cm to +3.3cm although the 23 stations spread over only a quarter of the SAR image frame (figure 2). Therefore, *it is crucial to apply such corrections in order for InSAR to achieve sub-centimetre accuracy.*

For each of the nine prediction sites shown in figure 2, the tropospheric delay corrections were interpolated using the three methods described earlier: inverse distance weighted (IDW) interpolation, spline interpolation and kriging interpolation. Both the single-differenced tropospheric corrections relative to CIT1 for days 214 and 249, and the double-differenced tropospheric corrections between these two epochs were investigated by comparing the interpolated values to the 'true' values obtained directly using the Bernese software. This was done for each of the six 20-minute time intervals (Delay 1 through to Delay 6) within the 2-hour observation span.

Figure 3 shows the interpolation images obtained for the kriging method in the double-differenced case, which is most important and can be directly used for the correction of InSAR results. The dots indicate the locations of the 22 GPS stations used in the analysis and the colour/grey step interval is 1mm. The main areas of tropospheric activity can be recognised in all of the plots, and the temporal and spatial variability of the tropospheric delay is obvious. The double-differenced interpolation values obtained with the different interpolation methods only differ by small amounts and are generally below or just above the cm-level. However, they *can* reach values of up to 3cm in some cases.

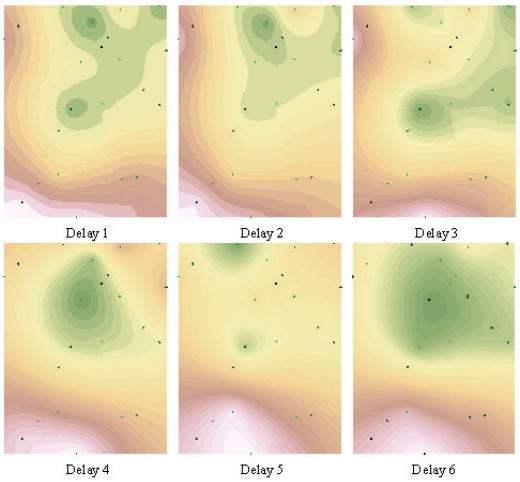

Figure 3. Interpolation images for double-differenced tropospheric corrections (Kriging).

In order to determine the reliability of interpolated results, the standard deviations of the results compared to the 'true' values obtained using the Bernese software were computed. Figure 4 shows the standard deviations for the single-differenced case on days 214 (top plot) and 249 (middle plot), as well as for the double-differenced case (bottom plot). It is obvious that all three interpolation techniques deliver results with the same accuracy in this particular case, which is mostly at the sub-centimetre

level. For the fourth time interval the accuracy is considerably lower compared to the rest of the observation span, almost reaching 2cm. This may have been caused by a short-term tropospheric event on day 249, which again highlights the importance of applying the differential tropospheric delay corrections to InSAR results.

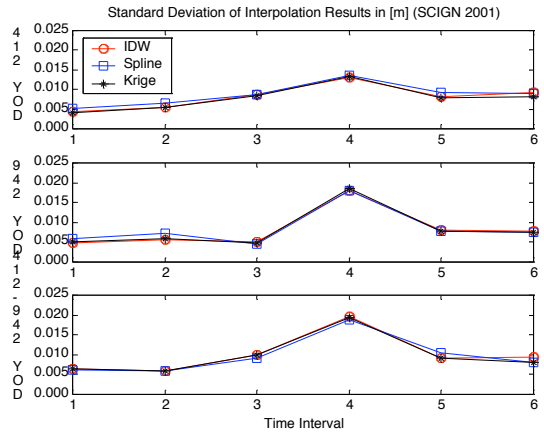

Figure 4. Standard deviation of the interpolation results obtained by different methods.

2.5 Experimental data analysis: GEONET

Based on the above findings a second dataset from Japan's GPS Earth Observation Network (GEONET) (GSI 2003) was analysed. Of the 37 stations considered, 29 were treated as measured locations (reference stations) and eight were used as prediction locations for which tropospheric delay corrections had to be determined and compared with their GPS-derived delays. A 2-hour session was observed on June 17, 2002 (DOY 168) and on July 22, 2002 (DOY 203), again simulating a typical ERS SAR satellite single repeat cycle of 35 days, and covering the satellite flyover epoch. Figure 5 shows the location of the GPS sites, evenly distributed across a typical ERS SAR image frame (the dashed lines) for this area. The reference stations are denoted by triangles, while the sites to be interpolated are indicated by circles. Precise coordinates for all sites were provided from the Geographical Survey Institute (GSI) of Japan.

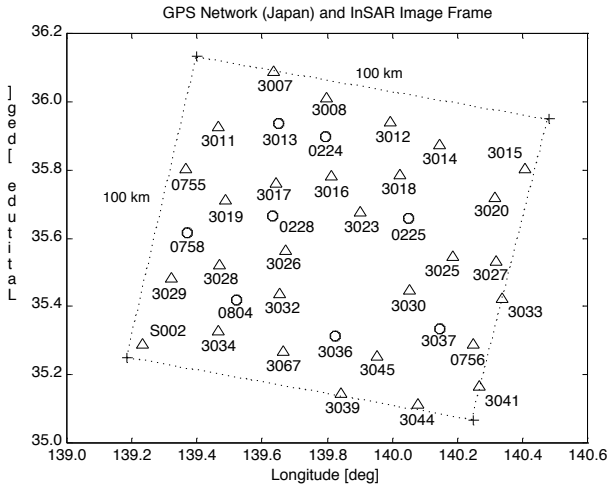

Figure 5. GEONET stations within the ERS SAR image frame.

Again, the Bernese GPS processing software was used to process the network data for both days, the coordinates of S002 being held fixed as the primary reference station. Baseline lengths vary from 22km to 121km, and the largest height difference is 321m. For each site tropospheric delay corrections were determined every 5 minutes, resulting in 24 parameters per site throughout the 2-hour observation span. It should be noted that in practice the primary reference station should be situated in, or close to, the centre of the SAR image frame in order to keep the baseline lengths to a minimum. In this analysis, however, the results obtained over longer baselines are also of interest.

Single-differenced tropospheric corrections (equation (1)) were determined by forming the differences relative to S002. These corrections range from –9.5cm to +4.2cm, showing variations of up to a few centimetres within the 2-hour observation span. Double-differenced tropospheric delay corrections were then obtained by forming the between-epoch difference of the single-differenced values derived in the previous step (equation (3)). The double-differenced corrections range from –6.7cm to +10.9cm, indicating significant changes in the tropospheric conditions (figure 6).

Figure 7 shows the double-differenced corrections for the eight prediction sites, obtained for each of the 24 time intervals. The graphs show the parameters determined by the Bernese software, the interpolated values using the IDW method, and the differences between the two. It can be seen that the interpolation results agree very well with the 'true' values. *The standard deviations of the differences are all (with one exception site 3013) at the sub-centimetre level, even for baselines of 85km in length (table 1).*

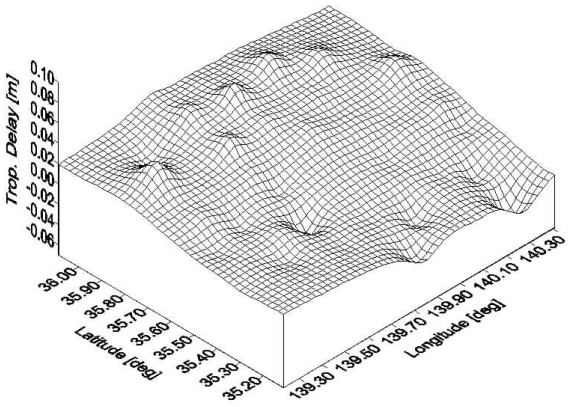

Figure 6. Double-differenced interpolation maps for the 11th time interval (IDW interpolation).

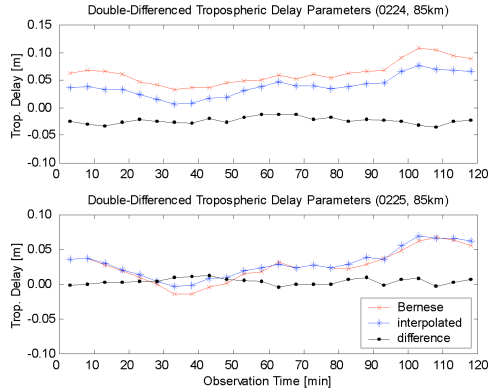

Figure 7. Comparison of Benese-derived and interpolated double-differenced tropospheric corrections.

Table 1. Standard deviations of the differences between Bernese-derived and interpolated troposphere corrections.

Site	STD [m]	Baseline length [km]
0224	0.00625	85
0225	0.00445	85
0228	0.00472	55
0758	0.00510	38
0804	0.00597	30
3013	0.01323	81
3036	0.00697	54
3037	0.00450	83

3. INTERPRETATION OF INSAR RESULTS WITH THE AID OF GIS

Ground subsidence is the lowering or collapse of the land surface, and is caused by a number of natural and human-induced activities. Most current subsidence is human-induced, and is related to underground mining activity or fluid extraction (oil and water pumping). In this section, we demonstrate how GIS can aid the interpretation of differential InSAR results obtained from monitoring subsidence due to underground coal mining.

3.1 Differential radar interferometry

Differential Interferometric Synthetic Aperture Radar (DInSAR) is a radar technique for detecting ground surface deformations by computing a differential interferogram of the same scene over two repeat-pass acquisitions which form a master-slave image pair (Massonnet et al., 1993). In total 29 and 42 pairs are chosen respectively from different combinations of 13 JERS-1 images (L-band) acquired during August 1993 and January 1996, and 18 ERS-1/2 images (C-band) acquired in the period from September 1995 to April 1997.

Figure 8 shows a differential result indicating the magnitude of the ground deformation during a period of 132 days between the master (9 November 1993) and slave (21 March 1994) acquisitions. The white spots show the locations of larger deformation with respect to other relatively small or zero ground elevation change areas (with darker grey scale). However, it is extremely hard to tell the geographic location of these subsidence regions with respect to ground features such as towns and rivers because the better a DInSAR result is, the less the topographic residual. Using radar image together with the subsidence image in the interpretation won't help much because radar image is a very poor portrait of the landscape compared to an aerial photo. GIS is an ideal tool to manage and process these data.

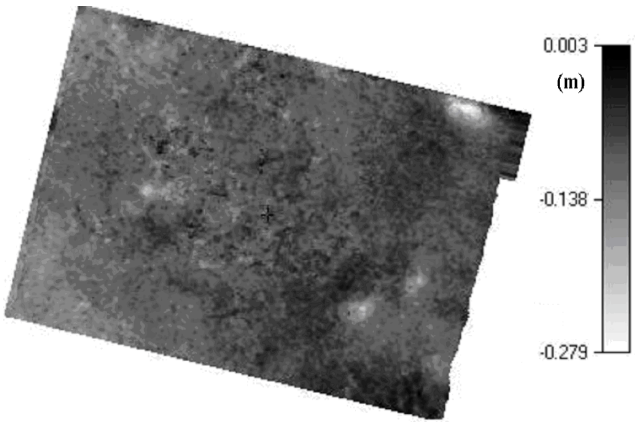

Figure 8. The differential InSAR height change results.

3.2 GIS-assisted analysis of differential InSAR results

Figure 9 shows an orthophoto of the mining sites, the layout of the mine plan (yellow/white) and a ground survey levelling line (black), all in GIS format provided by the company BHPBilliton.

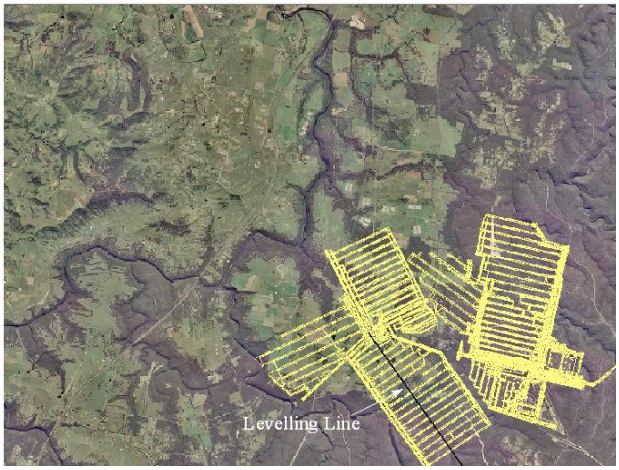

Figure 9. GIS data for the test site.

The differential InSAR results were exported to and post-processed in the GIS. The mine subsidence regions can now be seen clearly and the colour/grey coding indicates the magnitude of subsidence, as shown in Figure 10. A further advantage of using the GIS is that ground deformation can be analysed and visualised in various ways. For example, profiles can be generated along any lines across the subsidence area, in addition to along the gound survey line, as shown in Figure 11.

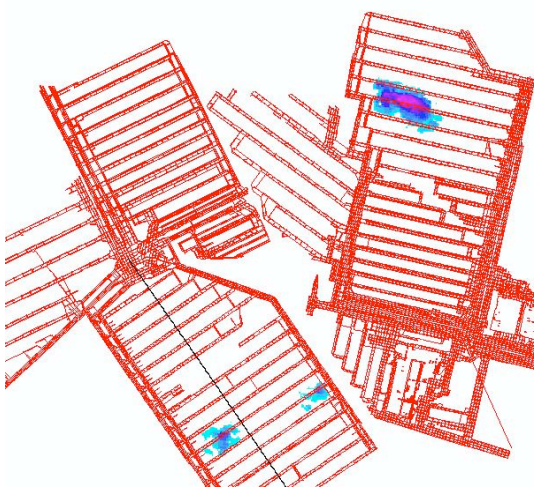

(a)

Figure 10. The result of figure 8 after post-processing using GIS tools.

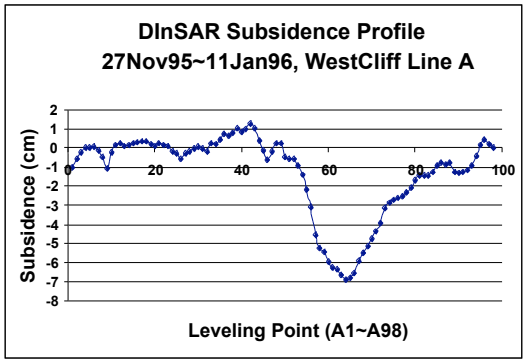

Figure 11. Profile covering both the deforming and stable regions derived from a DInSAR result.

Figure 11 shows a profile covering both the deforming (left-hand) and stable (right-hand) regions from a DInSAR result. The vertical axis is subsidence (in cm) while the horizontal axis the ground marks in the survey line. *The variation in the stable region is about +/-1cm, which demonstrates that DInSAR can resolve subsidence at the cm-level.*

Furthermore, the DInSAR derived subsidence can also be represented in many other forms such as a contour map (Figure 12a) and 3D perspective view (Figure 12b).

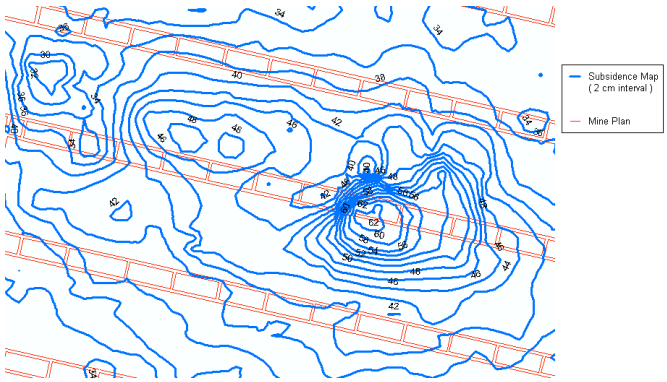

(a)

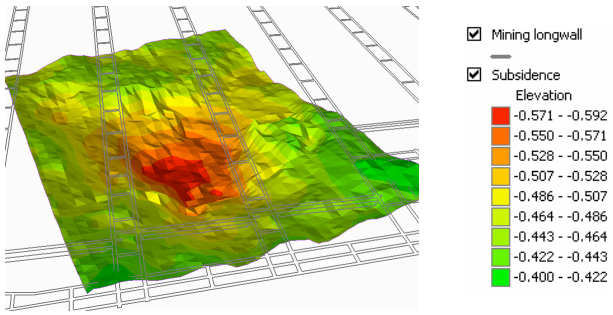

(b)

Figure 12. DInSAR-derived subsidence represented as (a) a contour map, and (b) in 3D view.

4. CONCLUDING REMARKS

Tropospheric heterogeneity (differential tropospheric delay) can lead to misinterpretation of InSAR results. A between-site and between-epoch double-differencing algorithm has been proposed to derive tropospheric corrections to radar results from GPS observations. These GPS measurements can be collected by either a network of continuous GPS (CGPS) stations or GPS campaigns synchronised to the radar satellite flyover. In order to correct the InSAR result on a pixel-by-pixel basis, the GPS-derived corrections have to be interpolated. Three interpolation methods, namely the inverse distance weighted, spline, and kriging techniques, have been investigated. Using GPS data from two test networks, it has been found that differential corrections as much as several centimetres may have to be applied and it has been demonstrated that the interpolation is reliable and can ensure sub-centimetre accuracy. The algorithm and procedures developed in this paper could easily be implemented in a CGPS network data centre. The interpolated grid of between-site, single-differenced tropospheric delays can be generated as a routine product to assist radar interferometry, in a manner similar to the SLC radar images.

With the assistance of GIS, several successful DInSAR results have been post-processed and have been used to demonstrate that the integration of satellite radar interferometry, GPS, and GIS can be used as an operational methodology to monitor, at cm-level resolution, ground subsidence due to activities such as underground mining. The operational procedures and tools have been developed and tested at the UNSW.

ACKNOWLEDGMENT

SCIGN and its sponsors, the W.M. Keck Foundation, NASA, NSF, USGS and SCEC, as well as Japan's Geographical Survey Institute are acknowledged for providing the GPS data used in this study. The authors wish to thank A/Prof Makoto Omura of Kochi Women's University, Japan, for providing L-band data, and ACRES (the Australian Centre for Remote Sensing) for providing C-band SAR images. The assistance of Yufei Wang and Lijiong Qin is gratefully acknowledged for the GIS analyses. The first author is supported by the Australian Research Council.

REFERENCES

Bernhardsen, T., 2002. *Geographic Information Systems – An Introduction,* 3rd edition, Wiley & Sons, Inc., New York, 428pp.

Bock, Y., et al., 1993. Detection of crustal deformation from the Landers earthquake sequence using continuous geodetic measurements, *Nature*, 361, 337-340.

Ge, L., 2000. *Development and Testing of Augmentations of Continuously-Operating GPS Networks to Improve Their Spatial and Temporal Resolution*, UNISURV S-63, The University of New South Wales, Australia.

GSI, 2003, http://mekira.gsi.go.jp/ENGLISH/index.html.

Lancaster, P., & Salkauskas, K., 1986. *Curve and surface fitting: An introduction*, Academic Press, London-Orlando.

Massonnet, D., Rossi, M., Carmona, C., Adragna, F., Peltzer, G., Feigl, K., & Rabaute, T., 1993. The displacement field of the Landers Earthquake mapped by radar interferometry, *Nature*, 364, 138-142.

Miyazaki, S., et al., 1996. Establishment of the nationwide GPS array and its initial results on the crustal deformation of Japan, *Bull. Geog. Surv. Inst. Jpn.,* 42, 27-41.

Rothacher, M., & Mervart, L., Eds, 1996, *Bernese GPS Software Version 4.0,* Astronomical Institute, University of Berne, Switzerland.

Schultz, M.H., 1973, *Spline Analysis*, Prentice-Hall Englewood Cliffs, N.J.

SCIGN, 2003, http://www.scign.org/.

Spilker, J.J., 1996, Tropospheric effects on GPS. In *Global Positioning System: Theory and applications* I, vol. 163, edited by B.W. Parkinson and J.J. Spilker, American Institute of Aeronautics and Astronautics, Washington, 517-546.

Stein, M.L., 1999, *Interpolation of Spatial Data: Some Theory for Kriging,* Springer, New York, 247pp.

Zebker, H.A., Rosen, P.A., & Hensley, S., 1997. Atmospheric effects in interferometric synthetic aperture radar surface deformation and topographic maps, *Journal of Geophysical Research*, 102(B4), 7547-7563.